AN EXPERIMENTAL AND COMPUTATIONAL STUDY OF BLUNT CAROTID ARTERY INJURY

F. Scott Gayzik[1,2], Ola Bostrom[3], Per Örtenwall[4], Stefan M. Duma[2], Joel D. Stitzel[1,2]

[1] Wake Forest University School of Medicine, Medical Center Blvd, Winston-Salem, NC 27157
[2] Virginia Tech – Wake Forest University Center for Injury Biomechanics, Medical Center Blvd, Winston-Salem, NC 27157
[3]Autoliv Research, 447 83 Vargarda, Sweden
[4]Sahlgrenska University Hospital, Gothenburg, Sweden

ABSTRACT

A carotid artery dissection begins as a tear or defect of the intimal lining of the artery, and can lead to luminal occlusion and ultimately cerebral ischemia. Our aim is to conduct an organ level validation of a finite element model of the carotid artery using an experiment designed to elicit internal layer failure within fluid-filled carotid artery samples. A 2.4-kg beveled guillotine is dropped from three heights (0.3, 0.5 and 0.7 m) onto fluid-filled porcine carotid arteries and resulting damage is recorded. These events are modeled using finite element analysis. Stress, strain and strain rate are correlated to experimental outcome. Internal layer damage is reported in half of the experiments, with damage occurring with 100% frequency at a drop height of 0.7 m. Simulations of this experiment result in maximum principal stress and strain values of 1.43 MPa and 46.2% respectively. The strain level predicted by the model for this impact scenario approaches the strain to intimal failure level for porcine arteries found in the literature. The results of this study represent an important step in validating this finite element carotid artery model at the organ level.

Through the collective efforts of clinicians, automotive safety researchers and legislators the rate of motor vehicle traffic-related injuries per 100 million vehicle miles traveled continues to drop (NHTSA 2003). Computational modeling continues to play an important role in engineering safety interventions. Recent research has focused on modeling injuries to specific soft tissue organs in the body including the brain (Zhang, Yang et al. 2001; Takhounts, Eppinger et al. 2003), lung (Stitzel, Gayzik et al. 2005), aorta (Shah,

Yang et al. 2001; Richens, Field et al. 2004), eye (Stitzel, Duma et al. 2002) and abdomen (Lee and Yang 2001).

Blunt or penetrating carotid artery injures are commonly encountered in automobile crashes (Stemper, Stineman et al. 2005; Stemper, Yoganandan et al. 2005). The associated mortality and long term neurological morbidity of this injury are estimated at 40% and 40-80% respectively (Stemper, Yoganandan et al. 2005). Among fundamental mechanisms of blunt carotid injury that have been identified, three constitute injury patterns associated with car crash; direct blow to the neck (e.g. seatbelt), hyperextension and contralateral rotation of the neck, and basilar skull fracture (Crissey and Bernstein 1974).

On a local level, Sinson et al. postulate that the main mechanism of injury is stretching of the artery secondary to neck extension (Sinson, Yoganandan et al. 2003). Others postulate direct blunt trauma to the neck is the mechanism for the injury. Rozycki et al., in a prospective study including 797 patients, found 16% sustained belt marks and of that 16%, 3% had sustained carotid artery injury. The study implicated belt loading as a direct cause of the cerebrovascular injuries (Rozycki, Tremblay et al. 2002). A similar conclusion was reached in a post-mortem case study of blunt carotid injury (Reddy, Furer et al. 1990). In summary, both blunt trauma (pinching) or distraction (tension) are likely causes of arterial injury.

The true incidence of this injury is unknown since many victims are not screened for injury, but blunt cerebrovascular injury (BCVI) is estimated to be present in roughly 1% of trauma admissions. By comparing two successive studies of this injury Miller et al. found that the incidence of BCVIs increased with aggressive screening (Miller, Fabian et al. 2001) (Miller, Fabian et al. 2002). Other studies identified similar trends, suggesting that BCVI has been historically under diagnosed (Biffl, Moore et al. 1998; Biffl, Moore et al. 2001).

The pathophysiology of BCVI begins as an intimal disruption. Such a disruption can ultimately lead to luminal narrowing via a number of different pathways including platelet aggregation, dissection of the intimal layer of the artery, aneurysm between interstitial layers, and intramural hematoma following hemorrhage of the vasa-vasorum (Biffl, Moore et al. 2001) (Schievink 2001; Haneline and Lewkovich 2005) (Haneline and Lewkovich 2005). Internal carotid artery dissection (ICAD) is 3 to 5 times as likely to occur as vertebral artery dissection, and more than 7000 cases of internal artery dissection per year occur in the United States alone (Schievink, Mokri et al. 1994; Haneline, Croft et al. 2003). A review of the available literature found that nearly 30% of all ICAD cases are attributed to some form of trauma (Haneline and Lewkovich 2005).

The internal branch of the left and right common carotid arteries, along with the vertebral arteries together are responsible for delivering 100% of the blood supplied to the brain. Disruptions in this blood supply lead to neurological deficit with devastating consequences. With a link between automobile crash and carotid artery injury (CAI) established, understanding the complex biomechanics of the carotid artery is critical to developing improved countermeasures.

Relative to the large body of work in the literature on modeling arteries at physiologic strain rates, there are few computational studies of their behavior during dynamic impact events. Several finite element analysis (FEA) studies have been published on traumatic aortic rupture (Shah, Yang et al. 2001; Richens, Field et al. 2004), however the authors are unaware of any study investigating traumatic injury mechanics of the carotid artery using FEA. The use of finite elements is a good approach for investigating high-rate arterial injury mechanisms since internal stress and strain values can be calculated provided that the model is sufficiently validated. Additionally, the finite element method is capable of modeling the complex morphology of structures like the carotid artery (Gayzik, Tan et al. 2006).

The philosophy the authors employ in developing the FE carotid artery model consists of validation at the tissue, organ and regional level. Tissue level validation consists of modeling a simple mechanical loading condition applied to a uniform sample (e.g. a uniaxial tension test). Validity of a material model is gained by comparing the results of a tissue level model to empirical uniaxial tension data. Following tissue level validation, modeling is conducted at the organ level. The purpose of organ level validation is to apply the material model developed at the tissue level to an isolated structure composed of that material undergoing a dynamic event. Upon completion of organ level validation, sufficient confidence in the model's ability to predict the mechanical behavior of the structure under study has been compiled such that the model can be implemented at a regional level.

Data on the failure mechanics of the porcine descending aorta (PDA) at quasi-static rates (Stemper, Stineman et al. 2005) were used for tissue level validation of this carotid artery model prior to commencement of this study. Simulated engineering stress vs. strain was highly correlated ($R^2 = 0.99$) with the experimental data. Our current aim is to use the FEA results to perform organ-level validation of the carotid artery model for later use in a regional level model of the neck.

This study has an experimental and computational component. In the experiment, excised porcine carotid arteries are struck with a semicircular (5 mm-radius) edged guillotine from three

drop heights. The purpose of this experiment is to expose intact carotid arteries to sufficient axial tension and "pinching" to elicit internal layer failure. The internal layer of the carotid arteries is assessed post-impact and coded as either injured or uninjured. Simulations of the guillotine experiments are then conducted using FEA and stress, strain and strain rate associated with this dynamic impact are calculated. Stress and strain values associated with internal layer failure found in the literature are used to compare the results of the FEA and the experiment, thereby assessing the organ-level validity of the model.

CERVICAL ARTERY ANATOMY

The portions of the left and right common carotid arteries traversing the neck (cervical portions) are anatomically identical. Cervical portions are subject to higher rates of injury than thoracic and cranial portions (Schievink 2001). At the level of C4, the artery bifurcates into the internal and external carotid arteries. The internal carotid artery (ICA) supplies blood to the brain, eye, nose and forehead.

The left and right vertebral arteries also traverse the neck superiorly. These arteries pass through the transverse foramina of the cervical vertebrae. While this may increase the risk of vertebral artery injury in the case of cervical vertebrae fractures or basilar skull fractures, this passage provides additional protection against blunt trauma not present for the carotid artery, which is surrounded by soft tissue rather than bone (Miller, Fabian et al. 2002). For this reason the analysis focuses on the carotid artery, although the structure of the arteries is similar.

The arteries are composed of three laminate layers, the intima, medial and adventitia. The intima lines the lumen of the artery and consists of endothelial cells and basal lamina. The thickness of this layer is roughly 80nm, although its composition and thickness will vary depending on the size of the vessel (Fung 1993). The media is composed of smooth muscle cells and various bundles of collagenous and elastic fibrils. The adventitia contains collagen fibers, basal lamina, blood vessels and nerves. Research on healthy, aged human external iliac arteries found that the ratio of the intimal-medial thickness to the adventitial thickness is on average 1:2 (Shulze-Bauer, et al. 2003). In the present study, arterial layers were not modeled individually, an approach used in prior vessel modeling (Shah, Yang et al. 2001).

METHODS

PART I: DYNAMIC IMPACT TESTS - Young porcine carotid arteries (aged 6 months or less) were harvested from an abattoir, and tested within 24 hours of acquisition. Vessels were

stored in a physiologic salt solution (0.9%). Immediately before testing the vessel was cut to size (mean axial length, 36 mm) and one end was tied shut. The other end was fixed to a cannula which filled the lumen to atmospheric pressure only. Filled arteries were placed in a semicircular notch within a polyethylene foam encasement. The notch was sized to accommodate the filled arteries snugly (mean filled diameter of the arteries was 5.1 ± 0.6 mm), and was sufficiently lubricated to reduce friction between the foam and the artery. The foam encasement above and below the artery was flat to ensure even contact as the foam was compressed by the indenter. The foam layers above and below the carotid artery were 14 mm and 25 mm thick respectively. Clear polycarbonate was placed flush to the encasement. The initial experimental protocol called for fixed end conditions, but no tension was observed during preliminary testing so free end conditions were used for all tests. Video of the impacting event was recorded at 1000 frames/sec. Arteries were tested once and a fresh sample was used for each test.

A 2.4-kg steel indenter, with 5 mm rounded tip at the impacting edge, was mounted on a vertically sliding guillotine and used to strike the samples. The indenter was released from three heights, striking the foam-encased artery perpendicularly at its midpoint. The drop heights of 0.3, 0.5 and 0.7 m above the sample resulted in impact speeds of 2.4, 3.1, and 3.7 m/s respectively. Two samples were tested at 0.3 m, and four were tested at the remaining two drop heights for a total of 10 tests. Figure 2 in the Results section shows a progression of the 0.5 m impact.

The carotid samples were subsequently removed from the foam encasement, cut along the longitudinal axis, and fixed in formalin. Internal layer integrity was assessed by visibly inspecting the lumen of the artery for fissures or tearing and outcome was coded as either damaged or undamaged. Histological analysis was not undertaken for reasons described in the Discussion. A post-impact prepared specimen is shown in Figure 3 of the results section. The experiment was conducted at Autoliv, and only samples from postmortem animals from an abattoir were used. No experimentation was conducted at Wake Forest University Baptist Medical Center and therefore no approval was sought at the medical center.

PART II: FINITE ELEMENT MODEL OF IMPACT - The finite element model was constructed from video of the experiment and is shown in Figure 1. The video of the experiment was split into an image stack where each frame of the video was a separate file (.tif). A frame prior to the impact was used to take vessel diameter and length measurements. Calibrated tape (1 cm increments) and a ruler were clearly visible in the frame enabling accurate calibration of measurements. Four diameter measurements were taken at discrete locations along the axis of the vessel and averaged. A single

measurement was taken to determine vessel length. Because vessel geometry varied little between tests, a single video was used to construct the model. The diameter and length used in the model were 4.5 mm and 30 mm respectively. The vessel diameter used in the model is within one standard deviation of the mean diameter calculated from analysis of five video files. The vessel length was slightly less than the mean axial length. However since all vessel damage observed in the experiment occurred directly below the indenter, vessel length was considered less critical than diameter. The reasonable assumption of circular cross section was made in creating the model.

To reduce computation time, two foam blocks were modeled instead of a single foam encasement with a semi-circular notch as was used in the experiment. Foam was modeled with 8-node hexahedral elements. The mesh of the top foam was tailored to accommodate large compressive strains. The indenter and the artery were constructed of quadrilateral shell elements. Vessel shell thickness was 0.5 mm. Meshing was accomplished using Finite Element Model Builder (FEMB, Livermore Software Technology Company, Livermore, CA). Lagrangian element formulations were used for all solid structures. A hexahedral Eulerian mesh surrounds the carotid artery and lower foam section to model the movement of the fluid within the carotid artery. The total number of elements in the model is 28196. The dynamic impact was analyzed using LS-Dyna (LSTC, Livermore, CA).

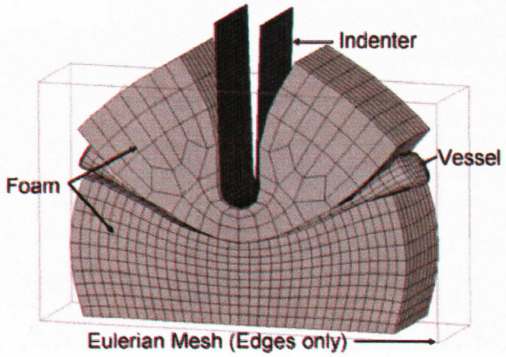

Figure 1. Finite element model of the dynamic porcine carotid tests, showing foam encasement, artery, indenter and boundary of the Eulerian flow field.

The foam was modeled using '*MAT_LOW_DENSITY_-FOAM' (*MAT_057). This foam is typically used in modeling seat cushions and side impact dummies (LSTC 2003). This model employs a user-provided stress-strain curve. The loading curve is used in the compressive regime to interpolate stresses from a calculated stretch. In the tensile regime the modulus of elasticity is used. The loading curve is nonlinear and taken the literature (Mills

and Masso-Moreu 2005). The Mills and Masso-Moreu stress vs. strain data result from drop testing of the same foam used in the present experiment. The material safety data sheet (MSDS) for the polyethylene foam provided nominal stress vs. strain data but only up to 50% compression. The literature data compared closely the MSDS data but extended out to full compression (99%). The modulus of elasticity was estimated from the slope of the compressive data.

The material model used for the carotid artery was *MAT_Simplified_Rubber (*Mat_181), a simplified model for modeling rubber-like materials under dynamic loading. The model is considered "simplified" because rather than providing coefficients for the underlying hyperelastic model (Ogden Model), the functional is computed for the uniaxial data provided (Du Bois 2003; Kolling, Du Bois et al. 2005). Uniaxial data is provided to the model in the form of stretch ratio (deformed length/undeformed length) and tensile force. Force deflection data from a quasi-static tensile test of young porcine descending aorta was used in the model (Stemper, Yoganandan et al. 2005).

The generalized form of the partial derivative of Ogden's hyperelastic strain energy density functional, with respect to the principal stretches λ is shown in Equation 1. In this equation, K is the bulk modulus, J is the volume ratio (V/V_o), λ^* is the modified stretch ratio ($\lambda^* = \lambda J^{1/3}$) and $f(\lambda)$ is a generalized function of Ogden coefficients. The simplified rubber model assumes a different form of $f(\lambda)$ than the conventional polynomial form (LSTC 2003). The alternative form of $f(\lambda)$ is shown in Equation 2. In this form, the uniaxial stress and strain data provided is used to directly calculate the function. Strain is calculated from the stretch ratio provided by the user via Equation (3) and the corresponding force is read from the uniaxial data. Stress is calculated by dividing the force by the undeformed specimen cross-sectional area.

$$\sigma_i = \frac{1}{J}\left(f(\lambda_i) - \frac{1}{3}\sum_{k=1}^{3} f(\lambda_i) \right) + K\frac{J-1}{J} \qquad (1)$$

$$f(\lambda_i) = \lambda_i \sigma_o(\varepsilon_{oi}) + \sum_{n=1}^{\infty} \lambda^{(1/2)^n} \sigma_o(\lambda^{(1/2)^n} - 1) \qquad (2)$$

$$\varepsilon_{oi} = \lambda_i - 1 \qquad (3)$$

The density of the carotid was taken as that of water. Bulk modulus was found in the literature (Duck 1991). Shear modulus was estimated from bulk modulus by assuming the carotid is nearly incompressible (Poisson's ratio of 0.499). A summary of the parameters used in the foam and carotid artery models is given in Table 1. The indenter was modeled as a rigid body.

Table 1. Parameters used in simplified rubber model of carotid artery

Porcine Carotid Artery	
Model	Simplified Rubber
Density, [g/mm^3]	1.00×10^{-3}
Bulk Modulus, [N/mm^2]	$2.71 \times 10^{+3}$
Shear Modulus, [N/mm^2]	5.20
Polyethylene Foam	
Model	Low Density Foam
Density, [g/mm^3]	36.0×10^{-6}
Elastic Modulus, [N/mm^2]	2.36×10^{-1}

Boundary conditions were set to mimic the experiment. The bottom most nodes of the foam were locked. Nodes on the edges of the foam were locked in-plane to mimic the presence of the polycarbonate sheet shown in Figure 2. The action of the simulation was modeled via a prescribed motion boundary condition applied to the indenter. The position of the indenter with respect to time was tracked for each drop height by importing the image stack created from video of the experiment into ImageJ (National Institutes of Health, http://rsb.info.nih.gov/ij/). Separate trajectories were applied as prescribed motion boundary conditions of the rigid indenter for a total of three simulations. Contact between Lagrangian solids was modeled using *Contact_Automatic_Single_Surface. Checks for initial nodal penetration from one part to a neighboring part were negative. Changes in shell thickness were included in the contact algorithm calculation. Stiffness type hourglass control was employed. Since little friction was observed in the experiment, friction between the foam and the vessel was not included.

Two procedures were conducted to give confidence to the results of the foam model; validation of the initial indenter velocity, and validation of the gross foam compression. The frame rate of 1000Hz was adequate to track the location of the indenter. Since the drop height of the indenter was carefully controlled in each case, the initial velocity was known via $v = \sqrt{(2*g*h)}$. By taking the derivative of the displacement history of the indenter a direct comparison was made to validate the initial velocity of the indenter. The second foam validation procedure was to compare the displacement of the lower foam surface of the simulation to that of the experiment. Simulated foam displacement was acquired by tracking the displacement of a node on the upper surface of the lower foam block. Displacements of the same point in the experiment were taken from video of the impacting event.

RESULTS

PART I: DYNAMIC IMPACT TESTS – Still frames from video of the impacting event are shown in Figure 2. Table 2 summarizes the results of the drop tests. Damage to the inside layer of the artery was assessed with the unaided eye, and was visible as a

distinct fissure on the lumen of the artery (Figure 3). In all tests where damage was present, the lesion occurred as a split with its long axis in the circumferential direction of the lumen and directly below the indenter. The intimal side of the artery was extremely delicate, and a lesion could be induced by simply pinching the artery. The incidence of injury increased with drop height, with 100% incidence of injury at 0.7 m. No damage was observed at 0.3 m.

Table 2. Summary drop test results

Height (m)	Number of tests	Penetration depth (mm)	Impact Speed (m/s)	Injury frequency
0.3	2	34	2.4	0%
0.5	4	36	3.1	25%
0.7	4	38	3.7	100%

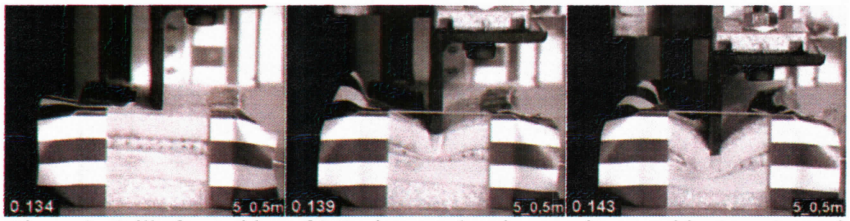

Figure 2. Stills from video of 0.5m impact showing porcine carotid artery encased in polyethylene foam and progression of indenter.

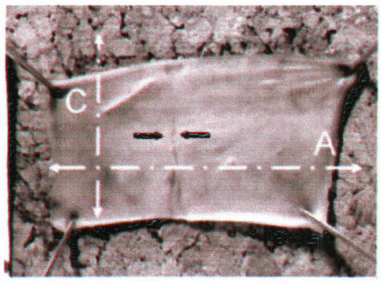

Figure 3. Post impact porcine carotid artery specimen with visible intimal damage (located by the black arrows). Circumferential and axial axes are also shown.

PART II: FINITE ELEMENT MODEL OF IMPACT – Despite some instability on initial runs the model performance was robust. Model instability was remedied by increasing the stiffness of the foam at very large strains (99.9%) and tailoring the mesh of the upper foam layer to accommodate large strains, Figure 1. A mesh convergence study was performed on the 0.7 m drop simulation wherein each element was split into either 4 or 8 elements (depending on whether the element was shell or brick). Peak stress and strain values resulting from the simulation were within 1% of the nominal mesh values. The hourglass energy in the vessel was low, (hourglass energy/internal energy ~ 2%) however was higher in the foam (ratio increased to 25%). More on the model numerical performance can be found in the discussion.

The foam validation procedures yielded positive results. The discrepancy between prescribed initial penetration velocity and calculated initial penetration velocity was less than 3% for all models. The lower foam displacement validation yielded high correlation for the 0.5 and 0.7 m drop simulations. The error between simulated and experimentally observed foam compression at max indenter penetration was less than 2% for both simulations. The 0.3 m simulation resulted in an error at max indenter penetration of 13%. Validation study results are summarized in Table 3 and Figure 4.

Table 3. Initial velocity validation data

Drop Height	Initial velocity (calculated)	Initial velocity (video)
0.3 m	2.42 m/s	2.51 m/s
0.5 m	3.13 m/s	3.13 m/s
0.7 m	3.70 m/s	3.69 m/s

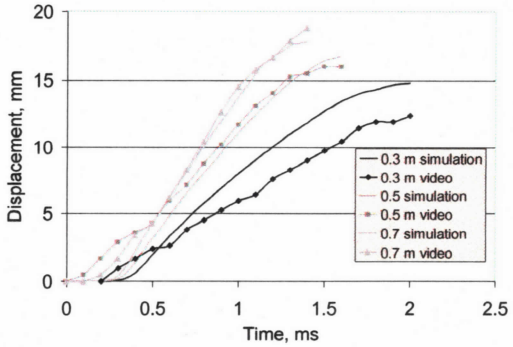

Figure 4. Results of the foam motion validation procedure. Experimental data are the location of the upper-edge the foam beneath the indenter. Simulation data are the location of the corresponding node.

Three regions of interest were defined to analyze the results of the finite element simulations (Figure 5). The top region contained 20 elements, 10 on either side of the vessel midline facing the upper foam, the bottom region mirrors the top region but faces the lower foam, and the side region contained a total of 24 elements (12 on each side). When summed, the surface area of the regions of interest covers a circumferential band about the vessel midline. Stress and strain within each region of interest were relatively uniform. Analysis of the impact event was performed by averaging the stress, strain and strain rate from each of these regions for each impact. All data was filtered using the built-in SAE filter in the post-processing software LS-PrePost (LSTC, Livermore, CA) and a cutoff frequency of 2000 Hz. Stress and strain values presented below are maximum principal stress and strain values (true stress and strain).

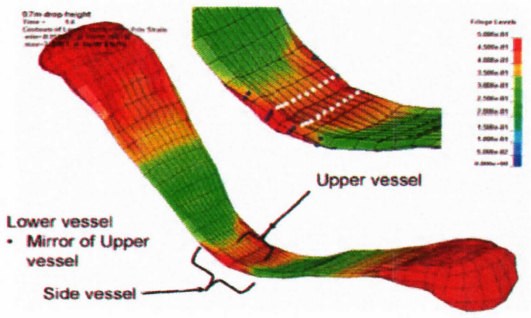

Figure 5. Regions of interest of the vessel. The upper vessel elements are denoted by white dots. The side region comprises two sets of elements denoted by dark dots, not all shown. No elements on the lower side of the vessel are visible, but they mirror the upper region.

In general, the stress and strain values occurring in the top and bottom regions were of greater magnitude than those occurring in the side region. For this reason, the analysis concentrates on the former two regions. The largest strains and strain rates occurred in the top region of the vessel. The same can not be said of the stresses, as the peak stresses were highest in the bottom region for the 0.5 and 0.7 m simulations. The difference between peak values in the top and bottom regions is within 10% in all cases, meaning the loading below the indenter was fairly uniform. Figure 6 shows the top side strain and stress resulting from each of the drop heights. A peak strain of 46% occurs in the 0.7 m simulation. This represents a 16% increase over the peak strain in the 0.3 m drop simulation. Strain rate values are fairly uniform. In the first 5 ms of the event, an average strain of 36% is achieved for all drop heights, correlating to an average strain rate of 73 strain•sec^{-1} ± 8.5 strain•sec^{-1}. Stress values increased more dramatically between drop heights than strain values. The peak stress on the section of the artery below the indenter increased 50% between the 0.3 m and 0.7 m drop, compared to an increase in stress of only 13.6% between the 0.3 m and 0.5 m drop. A summary of the strain, strain rate and stress from the simulations is provided in Table 4.

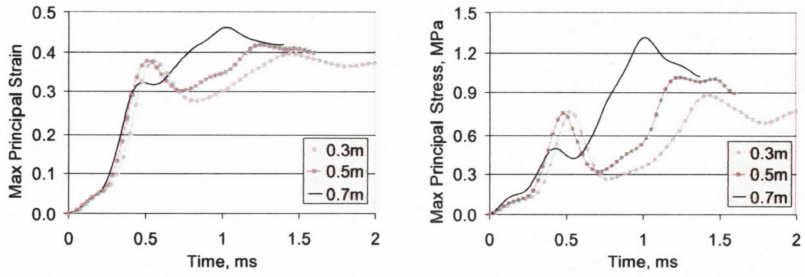

A. B.

Figure 6. Results from computational study. (A) First principal strain from top region for the three drop heights. (B) First principal stress from the same region for each drop height.

Table 4. Summary of strain, strain rate and stress values in drop simulations by region.

Height (m)	Vessel Region	5ms Strain rate (strain•sec-1)	Peak strain (%)	Peak stress (MPa)	Injury frequency (%)
0.3	Top	67.4	39.7	0.88	0
	Bottom	63.7	36.0	0.84	
0.5	Top	73.8	41.8	1.01	25
	Bottom	74.5	38.7	1.12	
0.7	Top	87.7	46.2	1.32	100
	Bottom	67.9	43.4	1.43	

A constraint placed on the Eulerian fluid bounded by the vessel ensured that the fluid remained inside the artery for the duration of the simulation. The models were investigated to verify that this constraint was obeyed throughout the simulation. Figure 7 shows plots of the fluid density for each of the three drop heights at the point of maximum indentation. The fluid density was $1 \cdot 10^{-3}$ $g \cdot m^{-3}$. Volume occupied by the fluid appears dark. Fringe levels are apparent as fluid approaches the edges of the Eulerian mesh. The images show that the fluid-in-solid constraint was maintained throughout the simulation. Fluid separation is noted at the maximum intrusion of the indenter in the 0.7 m simulation (Figure 7c).

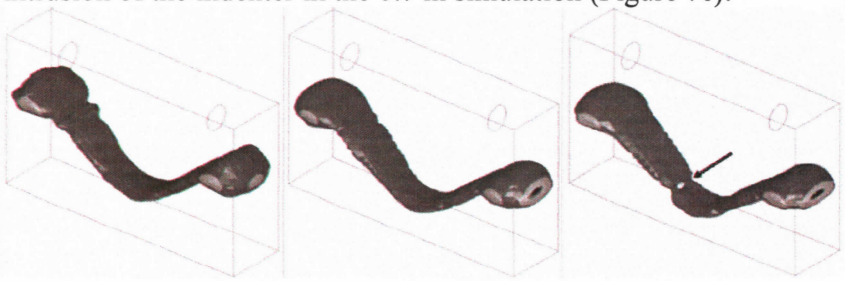

A. B. C.

Figure 7. Location of fluid within the carotid at point of furthest indentation. (A) 0.3m drop, 34 mm penetration; (B) 0.5 m drop, 36 mm penetration; (C) 0.7 m drop, 38 mm penetration. Arrow indicates location of fluid separation

This separation suggests that intima to intima contact is present at this drop height; however the lack of this phenomenon does not preclude top to bottom intimal contact. Figure 8 shows the relative distance between nodes at the upper-most and lower-most locations of the carotid artery. These nodes are precisely in the center of the model. The difference in their location gives an estimate of the distance between the upper and lower intimal layers. For all simulations the distance between nodes becomes progressively smaller as the indenter penetrates through the foam. Ultimately the distances cease to decrease, indicating that the upper and lower portions of the vessel are moving together and are in contact. The mean final separation value of the two sides of the vessel is 0.34 mm. Given the thickness of the shell (0.5 mm) it follows that the distance from the Gauss point of one shell to the closest Gauss point of an abutting but non-penetrating shell would be 0.211 mm. Therefore the final separation distance is slightly greater than the distance between Gauss points. This is not surprising since the location of the Gauss points do not coincide with the location of the nodes, and the final separation distance is a measure of nodal distance.

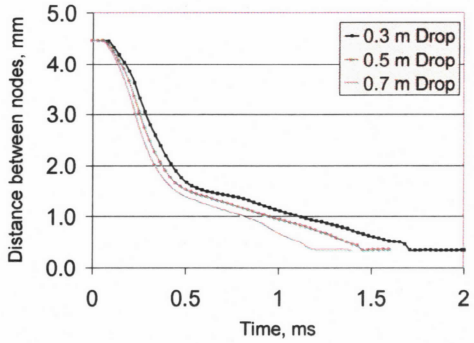

Figure 8. Distance between nodes at upper-most and lower-most points on the carotid artery at the midpoint.

DISCUSSION

The purpose of this study was to perform an organ level validation of a finite element model of the carotid artery for later use in a regional level model of the neck. This organ level validation study follows validation of the material model used for the carotid artery at the tissue level. The simulations show that all the mechanical values of interest increase between the 0.3 m and 0.7 m drops. Peak strain shows the lowest increase (16%) while the increase in peak stress is much greater.

The data used in development of the carotid artery model is the result of a study by Stemper, et al. characterizing the failure mechanics of the internal layer of the human carotid artery and

porcine descending aorta (PDA) (Stemper, Stineman et al. 2005). The authors of the latter study cut arterial samples into classic hourglass shaped mechanical test specimens and strained them to failure uniaxially at a quasi-static strain rate. Intimal failure was determined by videography. The authors of the present study chose to use the porcine data as the foundation for the human carotid artery model, following an observation made by Stemper et al. that young porcine descending aorta samples are likely to be a better surrogate for human arterial data. This observation is based on the following: fresh (not frozen or fixed) porcine samples are easily obtained. Young porcine samples (aged < 6mo.) are readily available whereas human arterial samples are typically of advanced age. The young arterial samples were also generally more elastic, exhibiting a greater strain to intimal failure than the human samples. Histological examination of the two samples found similar intimal pathology.

Converting observed failure values from Stemper et al. from engineering stress and strain to true stress and strain yields values of 2.0 MPa and 49% respectively. Despite observed intimal damage following 25% of the 0.5 m drop tests and 100% of the 0.7 m drop tests, the simulated stress (output from LS-Dyna is true stress) does not exceed this value in any of the simulations (see Table 4). However, the maximum strain resulting from the 0.7 m drop test (46%) approaches this value.

Strain to intimal failure may be a function of the strain rate in the vessel. It is well known that soft tissue is viscoelastic, exhibiting a rate dependent response to loading. The simulation indicates that the average strain rate in the first 5 ms of the guillotine test is 73 strain•sec^{-1}. This strain rate is in the range of previous injury biomechanics research investigating dynamic failure mechanics of arterial specimens. In their 1982 study, Mohan and Melvin used strain rates between 80 to 100 strain•sec^{-1} to investigate the failure properties of human aortic tissue. The investigators found that strain rate did not affect the ultimate strain of the aortic samples. However Mohan and Melvin were investigating ultimate stress not stress to intimal side at subfailure levels. Since Stemper et al. observed that intimal failure nearly always occurs prior to catastrophic failure, the Mohan and Melvin data is likely representative of the adventitial failure properties, and not necessarily those of the intima.

Heretofore, the discussion has centered on how the material characteristics of the vessel may have contributed to the incidence of luminal damage found in the experiments. However, intima to intima contact is another possible mechanism contributing to the 100% incidence of interior lumen damage following the 0.7 m drop. Fluid separation did not occur in the 0.3 m and 0.5 m drop simulations, but Figure 8 shows that contact is present in all simulations. The lumen of the samples was very delicate and could

certainly have been damaged by merely pinching the sides together. While this evidence alone is insufficient to implicate intima to intima contact as a mechanism of carotid artery injury, it is a clear demonstration of insight into the mechanics of the artery during a dynamic event that can only be gained through the use of FEA.

This conclusion shifts focus back to the testing method itself. The purpose of the experiment was to expose the carotid artery samples to sufficient axial tension and "pinching" to illicit internal layer failure. In real world crash scenarios, these two mechanical insults have been identified as mechanisms for carotid artery injury, with tension resulting from hyperextension of the neck and the "pinching" being associated with seat belt impingement on the neck. Clearly this test setup does not mimic the kinematics of the neck interacting with a seat belt, nor is it known how well the foam represents the soft tissue of the neck surrounding the carotid artery, however (and most importantly relative to this study), it is a repeatable test procedure for producing intimal side damage as a function of anvil drop height. The straightforward experimental design lends itself to computational investigation of the stress and strain experienced by the foam-encased artery and therefore is ideally suited for organ level model validation, the purpose of this study.

This organ level validation serves as an intermediate step between modeling the tissue level uniaxial tension tests and modeling the entire organ within a model of yet higher complexity (e.g. full neck model). While still more organ level validation may be required several important observations can be made from these initial simulations. First, the constitutive model of the artery based on uniaxial strain data seems to be a good choice for modeling the mechanical response of the artery. Care must be taken when using a curve fit model to ensure that model strain levels never exceed the maximum value of the stress vs. strain data provided to the model. Post-processing of the model demonstrated that this does not occur. The uniaxial data extends to roughly 55% strain (true), the point of catastrophic vessel failure. Model strains never exceeded 46% in the region below and near the indenter. Peak strain values in the artery for the most injurious drop test (0.7 m) approach strain values published in the literature for intimal side damage. The model is stable, exhibiting low hourglass energy despite large strains and strain rates. With regard to the elevated hourglass energy of the foam, the authors take the stance of previous researchers in the field who have cautioned against using elevated hourglass energy as a stand-alone indicator of model robustness (Takhounts et al. 2003). In our case, in the absence of any indication of model instability we consider the high hourglass to internal energy ratio in the foam a note of caution but not an indication of a serious flaw in the model.

The approach for modeling the fluid in the vessel was shown to be robust. The approach chosen uses LS-Dyna's fluid modeling algorithms employing Lagrangian and Eulerian elements simultaneously. The fluid modeling is based on an equation of state and does not employ full computational fluid dynamic (CFD) solutions. A CFD approach to the problem would add to the computational cost, and the purpose of this study is not to investigate what is happening mechanically within the fluid but to replicate the experimental conditions, and to investigate the mechanics of the artery itself under high rate, and large deformations. The same modeling technique has been used previously in injury biomechanics research in developing a nonlinear model of the eye for investigating globe rupture (Stitzel, Duma et al. 2002).

The experiment used in this organ-level validation study leads to some limitations on the results. The experimental design precludes validation of arterial strains beneath the indenter via tracking markers on the adventitial side. However, with tissue level validation completed prior to this study and with the foam and indenter motion validated against video of the experiment, the strain values calculated in the model are considered valid. Another potentially contentious point of the experiment is the use of a 5 mm beveled indenter in the tests. The experiment was not designed to recreate conditions experienced by a vehicle occupant in any particular crash mode. However it is a repeatable means to creating tensile and pinching loading mechanisms that while exaggerated may be considered "worst case" loading. Specifically regarding the indenter, since a fabric belt will not support compression or bending, in a dynamic event where belt contact on the neck occurs, the authors postulate that the belt may fold back onto itself as the tensile load increases. This folding or "roping" would result in a semicircular shape of relatively small radius, which the authors feel is reasonably represented by the beveled indenter. Roping is generally associated with the lap belt.

A subtle but important aspect of this study is the coding of damage to the inner layer of the artery without using histology. The authors acknowledge that damage to the lumen of the artery characterized as purely intimal would be impossible to determine with the unaided eye. The intima is an extremely thin cellular layer of the vessel wall and microscopic analysis would be required to detect deficits in this layer resulting from testing. However, damage to the intimal side characterized by disruption of the entire intima and a portion of the remaining layers is discernible. We refer again to the work of Stemper et al. (Stemper et al. 2005). In this work, arterial subfailure was correlated to a stress and strain state via videography, not histological analysis. Since we employ data from these tests in our material model, the aim of the study was to use the

FE model results to predict the same type of damage, sub-catastrophic failure involving both the intima and a portion of the remaining vessel wall. The investigation of purely intimal vessel failure is an interesting topic and may be a matter for future research.

A number of researchers have investigated arterial mechanics of the individual layers (Shulze-Bauer, et al. 2003; Fung, 1993). Fung tested specimens of porcine thoracic aorta under bending to determine the mean value of Young's modulus (stiffness) for the intima-media layer and the adventitial layer. His analysis showed that in general, the intimal-medial layer was significantly stiffer than the adventitial layer. Holfzapel et al. described a method to test all three arterial layers individually under quasi-static uniaxial loading by separating layers with a scalpel prior to testing, and reported that the intima is the stiffest layer over the whole domain (Holzapfel, Sommer et al. 2005). This testing however was performed on postmortem human left anterior descending coronary artery samples which have exhibited remarkable intimal thickening. The intima alone in this study was reported as 27% of the total wall thickness. Therefore it is likely that the microscopic composition of what Holzapfel regarded as intima bears little resemblance to healthy intima lining large vessels like the carotid.

Qualitatively, the above findings support the notion that intimal sub failure will nearly always occur prior to catastrophic vessel failure since the adventitia was found to be more compliant than the inner layers. However the data is insufficient for developing finite element models. In the case of the Fung data, only elastic moduli were calculated and in the case of the Holzapfel data, specimen quality is questionable. To the author's knowledge, the uniaxial data from the literature we have employed in tissue level and organ level validation of the carotid artery model is the only data set available that directly links stress and strain values to internal layer failure.

CONCLUSION

We have presented a computational and experimental study on the organ level validation of a fluid filled carotid artery model. The carotid artery model was developed using a simplified rubber model and employs both Lagrangian and Eulerian element formulations. Intimal-medial damage was found with 100% frequency following a drop of a 2.4 kg indenter from a height of 0.7 m. Simulations of this experiment result in maximum true strain levels beneath the indenter of 46%, a value that approaches published data on strain to internal layer failure. The simulations indicate that strain rates as high as 73 strain•sec^{-1} are experienced by the vessel during the event, and that intima to intima contact may have played a role in the frequency of observed damage in the experiment. Insights

gained from this organ level validation will ultimately be used towards the development of a regional level model of the neck.

ACKNOWLEDGEMENTS

The authors gratefully acknowledge Dr. Brian Stemper and Dr. Frank Pintar of the Department of Neurosurgery, Medical College of Wisconsin for the use of data on the failure mechanics of the porcine descending aorta originating from their labs.

The funding for this research has been provided in part by an Australian Research Council linkage grant and by private parties, who have selected Dr. Kennerly Digges and FHWA/NHTSA National Crash Analysis Center at the George Washington University to be an independent solicitor of and funder for research in motor vehicle safety, and to be one of the peer reviewers for the research projects and reports. Neither of the private parties have determined the allocation of funds or had any influence on the content of this report. This research was also supported in part by the Department of Veterans Affairs Medical Research.

REFERENCES

American Heart Association Heart Disease and Stroke Statistics – 2005 Update. Dallas, TX. American Heart Association ; 2005

Biffl, W. L., E. E. Moore, et al. (2001). "Blunt carotid and vertebral arterial injuries." World J Surg **25**(8): 1036-43.

Biffl, W. L., E. E. Moore, et al. (1998). "The unrecognized epidemic of blunt carotid arterial injuries: early diagnosis improves neurologic outcome." Ann Surg **228**(4): 462-70.

Crissey, M. M. and E. F. Bernstein (1974). "Delayed presentation of carotid intimal tear following blunt craniocervical trauma." Surgery **75**(4): 543-9.

Du Bois, P. (2003). A simplified approach for the simulation of rubber like materials under dynamic loading. 4th European LS-DYNA User's Conference, D-I-31/46.

Duck, F. A. (1991). Physical Properties of Tissue, A comprehensive reference book. London, Academic Press.

Fung, Y. (1993). Biomechanics - Mechanical property of living tissue. New York, Springer.

Gayzik, F., J. Tan, et al. (2006). Mesh development for a finite element model of the carotid artery. Biomedical Sciences Instrumentation Rocky Mountian Bioengineering Symposium, Terre Haute, IN.

Haneline, M. T., A. C. Croft, et al. (2003). "Association of internal carotid artery dissection and chiropractic manipulation." Neurologist **9**(1): 35-44.

Haneline, M. T. and G. N. Lewkovich (2005). "An analysis of the etiology of cervical artery dissections: 1994 to 2003." Journal of Manipulative and Physiological Therapeutics **28**(8): 617-622.

Holzapfel, G. A. (2006). "Determination of material models for arterial walls from uniaxial extension tests and histological structure." Journal of Theoretical Biology **238**(2): 290-302.

Holzapfel, G. A., G. Sommer, et al. (2005). "Determination of layer-specific mechanical properties of human coronary arteries with nonatherosclerotic intimal thickening and related constitutive modeling." Am J Physiol Heart Circ Physiol **289**(5): H2048-2058.

Kolling, S., P. Du Bois, et al. (2005). A simplified rubber model with damage. LS-DYNA Anwenderforum, Bamberg.

Lee, J. and K. Yang (2001). "Development of a finite element model of the human abdomen." Stapp Car Crash Journal **45**: 79-100.

LSTC (2003). LS-Dyna Keyword User's Manual, Livermore Software Technology Corporation, April 2003, v. 970.

Miller, P. R., T. C. Fabian, et al. (2001). "Blunt cerebrovascular injuries: diagnosis and treatment." J Trauma **51**(2): 279-85; discussion 285-6.

Miller, P. R., T. C. Fabian, et al. (2002). "Prospective screening for blunt cerebrovascular injuries: analysis of diagnostic modalities and outcomes." Ann Surg **236**(3): 386-93; discussion 393-5.

Mills, N. J. and Y. Masso-Moreu (2005). "Finite Element Analysis (FEA) Applied to Polyethylene Foam Cushions in Package Drop Tests." Packaging Technology and Science **18**: 29-38.

NHTSA (2003). National overview of recent highway safety data. N. H. T. S. Administration.

Reddy, K., M. Furer, et al. (1990). "Carotid artery dissection secondary to seatbelt trauma: case report." J Trauma **30**(5): 630-3.

Richens, D., M. Field, et al. (2004). "A finite element model of blunt traumatic aortic rupture." European Journal of Cardio-Thoracic Surgery **25**(6): 1039-1047.

Rozycki, G. S., L. Tremblay, et al. (2002). "A prospective study for the detection of vascular injury in adult and pediatric patients with cervicothoracic seat belt signs." J Trauma **52**(4): 618-23; discussion 623-4.

Schievink, W. I. (2001). "Spontaneous dissection of the carotid and vertebral arteries." N Engl J Med **344**(12): 898-906.

Schievink, W. I., B. Mokri, et al. (1994). "Recurrent spontaneous cervical-artery dissection." N Engl J Med **330**(6): 393-7.

Shah, C., K. Yang, et al. (2001). "Development of a computer model predict aortic rupture due to impact loading." Stapp Car Crash Journal **45**: 161-182.

Sinson, G. P., N. Yoganandan, et al. (2003). Carotid artery trauma in motor vehicle crashes: Investigation of the local tensile mechanism. IRCOBI Conference, Lisbon, Portugal.

Stemper, B. D., M. R. Stineman, et al. (2005). Mechanical Characterization of Internal Layer Failure in the Human Carotid Artery. IRCOBI, Prauge, Czech Republic.

Stemper, B. D., N. Yoganandan, et al. (2005). "Methodology to study intimal failure mechanics in human internal carotid arteries." J Biomech **38**(12): 2491-6.

Stitzel, J., S. Duma, et al. (2002). "A nonlinear fnite element model of the eye with experimental validation for the prediction of globe rupture." Stapp Car Crash Journal **46**: 243-265.

Stitzel, J., F. Gayzik, et al. (2005). "Development of a finite element based injury metric for pulmonary contusion, Part I: model development and validation." Stapp Car Crash Journal **49**: 271-289.

Takhounts, E., R. Eppinger, et al. (2003). "On the development of hte SIMon finite element head model." Stapp Car Crash Journal **47**: 107-133.

Zhang, L., K. Yang, et al. (2001). "Recent advances in brain injury research: A new human head model development and validation." Stapp Car Crash Journal **45**: 369.